Numerical Modeling of the Nonlinear Elastic Response of Filled Elastomers via Composite-Sphere Assemblages

Taha Goudarzi
e-mail: goudarz2@illinois.edu

Oscar Lopez-Pamies
e-mail: pamies@illinois.edu

Department of Civil
and Environmental Engineering,
University of Illinois Urbana–Champaign,
IL 61801-2352

This paper proposes an effective numerical method to generate approximate solutions for the overall nonlinear elastic response of isotropic filled elastomers subjected to arbitrarily large deformations. The basic idea is first to idealize the random microstructure of isotropic filled elastomers as an assemblage of composite spheres and then to generate statically admissible numerical solutions, via finite elements, for these material systems directly in terms of the response of a single composite sphere subjected to affine stress boundary conditions. The key theoretical strengths of the method are discussed, and its accuracy and numerical efficiency assessed by comparisons with corresponding 3D full-field simulations. The paper concludes with a discussion of straightforward extensions of the proposed method to account for general classes of anisotropic microstructures and filler-elastomer interphasial phenomena, features of key importance in emerging advanced applications. [DOI: 10.1115/1.4023497]

Keywords: finite strain, hydrodynamic reinforcement, energy methods

1 Introduction

The addition of filler particles to elastomers, even in small amounts, is known to greatly improve the stiffness—as well as many other mechanical/physical properties—of this increasingly pervasive class of materials [1]. Among the various microscopic mechanisms that are responsible for such strong stiffening, in this work we shall focus primarily on the so-called "hydrodynamic reinforcing" effect within the context of nonlinear elastic deformations. That is, we view filled elastomers as two-phase particulate composites—comprising a continuous elastomeric matrix reinforced by a statistically uniform distribution of disconnected inclusions firmly bonded across interfaces—and study their macroscopic (or overall) elastic response, which, roughly speaking, is expected to be some weighted average of the elastic response of the elastomeric matrix and the comparatively rigid response of the fillers.

The first microscopic theoretical studies of the overall linear elastic response of filled elastomers date back to the 1940s [2,3], but it was not until the 1970s that a formal framework for describing their overall nonlinear elastic response at *finite deformations* was put forward [4]. At any rate, because of the *constitutive nonconvexity* and *nonlinear incompressibility constraint* inherent of elastomers, the application of this framework to generate rigorous results for specific problems has proved remarkably challenging, especially in 3D. Indeed, it is only recently that a few rigorous results have been worked out (see for instance Ref. [5] and references therein).

In this paper, we put forward an effective numerical method to generate approximate solutions for the overall nonlinear elastic response of filled elastomers subjected to arbitrarily large deformations. The basic idea corresponds essentially to a generalization of the "composite-sphere-assemblage" approach of Hashin [6] to the nonconvex realm of finite elasticity[1]. More specifically, as elaborated in Sec. 3, the strategy is first to idealize the random microstructure of filled elastomers as an assemblage of homothetic composite spheres. And then to generate a variational *statically admissible* solution for the overall nonlinear elastic response of these material systems directly in terms of the response of a single composite sphere subjected to affine stress boundary conditions. While the elastostatics problem of a composite sphere subjected to affine stresses cannot be solved by analytical means, as detailed in Sec. 4, it is a simple matter to perform the relevant calculations numerically with finite elements (FE). The key theoretical strengths of this method are discussed in Sec. 3.2. Sample applications to various elastomeric materials, concentrations of particles, and loading conditions together with comparisons with corresponding 3D full-field simulations are provided in Sec. 5 to assess its accuracy and numerical efficiency. Finally, Sec. 6 provides an outline of extensions of the proposed method to account for general classes of anisotropic microstructures and filler-elastomer interphasial phenomena, features of key importance in emerging advanced applications (see, e.g., Refs. [8,9]).

2 The Problem

Consider a filled elastomer comprising a continuous matrix reinforced by a random distribution of firmly bonded particles that occupies a domain Ω, with boundary $\partial\Omega$, in its undeformed stress-free configuration. The matrix is labeled as phase $r=1$, while the particles are collectively identified as phase $r=2$. The domains occupied by each individual phase are denoted by $\Omega^{(r)}$ so that $\Omega=\Omega^{(1)}\cup\Omega^{(2)}$. It is assumed that the characteristic size of the particles is much smaller than the size of Ω, and that their spatial distribution is statistically uniform.

Material points in the solid are identified by their initial position vector $\mathbf{X}$ in Ω. Upon deformation the position vector of a point in the deformed configuration Ω' is specified by $\mathbf{x}=\boldsymbol{\chi}(\mathbf{X})$, where $\boldsymbol{\chi}$ is a continuous and one-to-one mapping from Ω to Ω'. The pointwise deformation gradient tensor is denoted by $\mathbf{F}=\mathrm{Grad}\boldsymbol{\chi}$.

Both the matrix ($r=1$) and the particles ($r=2$) are taken to be nonlinear elastic solids characterized by nonnegative, objective, and quasi-convex stored-energy functions $W^{(r)}$ of the deformation

[1] An extension of this approach to nonlinear, though convex, problems appears to have been first carried out by Barrett and Talbot [7] in the context of two-phase dielectrics.

Manuscript received July 21, 2012; final manuscript received January 18, 2013; accepted manuscript posted January 28, 2013; published online July 19, 2013. Assoc. Editor: Martin Ostoja-Starzewski.

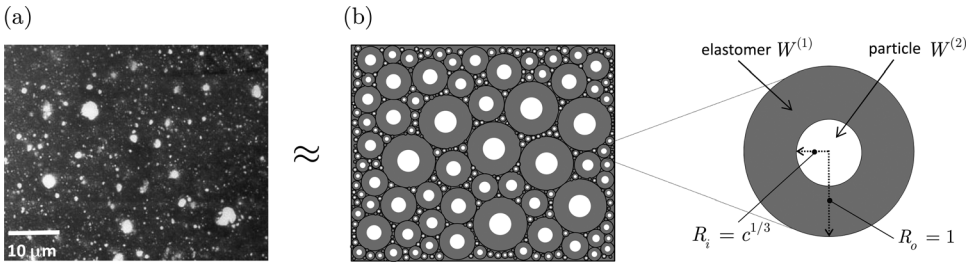

Fig. 1 (*a*) Electron micrograph of a styrene-butadiene rubber filled with an isotropic distribution of silica particles [14] and (*b*) its idealization as a composite-sphere assemblage (CSA) in the undeformed configuration. All the composite spheres in the assemblage are homothetic in that they have the same ratio of inner-to-outer radius $R_i/R_o = c^{1/3}$.

gradient $\mathbf{F}$, which linearize properly in the limit of small deformations as $\mathbf{F} \to \mathbf{I}$. At each material point $\mathbf{X}$ in the undeformed configuration, the first Piola–Kirchhoff stress $\mathbf{S}$ is, thus, related to $\mathbf{F}$ via

$$\mathbf{S} = \frac{\partial W}{\partial \mathbf{F}}(\mathbf{X},\mathbf{F}), \quad W(\mathbf{X},\mathbf{F}) = (1-\theta(\mathbf{X}))\ W^{(1)}(\mathbf{F}) + \theta(\mathbf{X})\ W^{(2)}(\mathbf{F}) \tag{1}$$

where the indicator function θ is equal to 1 if the position vector $\mathbf{X}$ is inside a particle and zero otherwise. The volume average of θ over Ω corresponds to the initial volume fraction or concentration of particles, which we denote by

$$c \doteq \frac{|\Omega^{(2)}|}{|\Omega|} = \frac{1}{|\Omega|}\int_\Omega \theta(\mathbf{X})\mathrm{d}\mathbf{X} \tag{2}$$

Granted the hypotheses of separation of length scales and statistical uniformity of the microstructure together with the constitutive quasi-convexity of W, the overall or macroscopic constitutive response for the above-described reinforced solid is defined as the relation between the volume averages of the first Piola–Kirchhoff stress $\overline{\mathbf{S}} \doteq |\Omega|^{-1}\int_\Omega \mathbf{S}(\mathbf{X})\mathrm{d}\mathbf{X}$ and the deformation gradient $\overline{\mathbf{F}} \doteq |\Omega|^{-1}\int_\Omega \mathbf{F}(\mathbf{X})\mathrm{d}\mathbf{X}$ when the material is subjected to affine boundary conditions [4]. In the case of affine deformations

$$\mathbf{x} = \overline{\mathbf{F}}\mathbf{X} \quad \text{on} \quad \partial\Omega \tag{3}$$

and the derivation of the overall response reduces to finding $\overline{\mathbf{S}}$ for a given $\overline{\mathbf{F}}$. For affine stresses, on the other hand,

$$\mathbf{S}\mathbf{N} = \overline{\mathbf{S}}\mathbf{N} \quad \text{on} \quad \partial\Omega \tag{4}$$

with $\mathbf{N}$ denoting the outward normal to the boundary, and the derivation reduces to finding $\overline{\mathbf{F}}$ for a given $\overline{\mathbf{S}}$. In either case, the result can be expediently written as [10]

$$\overline{\mathbf{S}} = \frac{\partial \overline{W}}{\partial \overline{\mathbf{F}}}(\overline{\mathbf{F}}, c) \tag{5}$$

where the scalar-valued function

$$\overline{W}(\overline{\mathbf{F}}, c) \doteq \min_{\mathbf{F}\in\mathcal{K}} \frac{1}{|\Omega|}\int_\Omega W(\mathbf{X},\mathbf{F}) \quad \mathrm{d}\mathbf{X} \tag{6}$$

corresponds physically to the total elastic energy per unit undeformed volume stored in the material; in this last expression, $\mathcal{K}$ denotes a sufficiently large set of kinematically admissible deformation gradient fields with prescribed volume average $\overline{\mathbf{F}}$. An analogous description in terms of a complementary energy is possible, but that route requires the use of multivalued functions that complicate unnecessarily the analysis (see, e.g., Refs. [11,12]; Chapter 5.4 in Ref. [13]).

The foregoing formulation for the overall finite-deformation response of filled elastomers is valid for any distribution of the underlying reinforcing particles. In the sequel, the focus shall be on the physically relevant case of *isotropic* distributions, but the case of anisotropic distributions is also briefly discussed.

3 Approximate Solution for Isotropic Distributions of Particles

3.1 Idealization of the Microstructure as a Composite-Sphere Assemblage. Figure 1(*a*) shows an electron micrograph of a synthetic rubber filled with an isotropic distribution of silica particles [14]. As is the case with other standard reinforcing fillers, the silica particles are seen to agglomerate into "particles" of roughly spherical shape and many different (i.e., polydisperse) sizes [1]. Based on this observation, our first step to construct a solution for the overall nonlinear elastic response of isotropic filled elastomers—as characterized by the effective stored-energy function (6)—is to idealize their microstructures as a composite-sphere assemblage (CSA). Figure 1(*b*) depicts schematically the polydisperse nature of the CSA and the fact that the concentration of particle in each composite sphere is equal to the concentration of particles c in the entire assemblage since all the composite spheres have identical ratios of inner-to-outer radius; the interested reader is referred to Chapter 7 in Ref. [15] for further properties of CSAs.

The exact computation of the overall nonlinear elastic response of a CSA is as difficult as that of any real microstructure. Unlike real microstructures, however, CSAs allow for the construction of variational approximations for their effective stored-energy function (6) based on *nonuniform* admissible trial fields, hence, providing the means to account for higher microstructural information beyond merely the concentration of particles.

3.2 Variational Approximation for the Response of a CSA. Having idealized the microstructures of isotropic filled elastomers as a CSA, we now turn to constructing a variational statically admissible[2] approximation for their effective stored-energy function $\overline{W}$ under arbitrarily large deformations. We begin by introducing the Legendre transformation:

$$W^*(\mathbf{X},\mathbf{P}) = \sup_{\mathbf{F}}\{\mathbf{P}\cdot\mathbf{F} - W(\mathbf{X},\mathbf{F})\} \tag{7}$$

A direct consequence of this definition is that, for any $\mathbf{P}$ and $\mathbf{F}$,

$$W(\mathbf{X},\mathbf{F}) \geq \mathbf{P}\cdot\mathbf{F} - W^*(\mathbf{X},\mathbf{P}) \tag{8}$$

and, hence, that

[2]The analogous kinematically admissible approximation is discussed in the Appendix.

$$\overline{W}(\overline{\mathbf{F}},c) \geq \min_{\mathbf{F}\in\mathcal{K}(\overline{\mathbf{F}})} \frac{1}{|\Omega|}\int_\Omega \mathbf{P}\cdot\mathbf{F}\mathrm{d}\mathbf{X} - \frac{1}{|\Omega|}\int_\Omega W^*(\mathbf{X},\mathbf{P})\mathrm{d}\mathbf{X}. \quad (9)$$

For the inequality (9) not to be trivial, the field $\mathbf{P}$ needs to be selected divergence-free, in which case it follows from Hill's lemma that

$$\overline{W}(\overline{\mathbf{F}},c) \geq \overline{\mathbf{P}}\cdot\overline{\mathbf{F}} - \frac{1}{|\Omega|}\int_\Omega W^*(\mathbf{X},\mathbf{P})\mathrm{d}\mathbf{X} \quad (10)$$

where the notation

$$\overline{\mathbf{P}} \doteq \frac{1}{|\Omega|}\int_\Omega \mathbf{P}(\mathbf{X})\mathrm{d}\mathbf{X} \quad (11)$$

has been introduced for convenience. In view of the definition (7), the inequality (10) can be written more explicitly as

$$\overline{W}(\overline{\mathbf{F}},c) \geq \frac{1}{|\Omega|}\int_\Omega W(\mathbf{X},\mathbf{F}^S)\mathrm{d}\mathbf{X} + \overline{\mathbf{P}}\cdot\overline{\mathbf{F}} - \frac{1}{|\Omega|}\int_\Omega \mathbf{P}\cdot\mathbf{F}^S\mathrm{d}\mathbf{X} \quad (12)$$

with the second-order tensor $\mathbf{F}^S$ being implicitly defined in terms of $\mathbf{P}$ as the solution to the algebraic equation

$$\mathbf{P} - \frac{\partial W}{\partial \mathbf{F}}(\mathbf{X},\mathbf{F}^S) = 0 \quad (13)$$

that maximizes the right-hand side of (7); note that $\mathbf{F}^S$ does not necessarily correspond to the gradient of a deformation field.

The inequality (12) is valid for any choice of microstructure (i.e., any indicator function θ) and any choice of divergence-free field $\mathbf{P}$. At this point, we exploit the fact that the microstructure under study here is a CSA and consider divergence-free fields $\mathbf{P}$ that satisfy the affine condition

$$\mathbf{PN} = \overline{\mathbf{P}}\mathbf{N} \quad (14)$$

on the surface of each composite sphere in the assemblage. By virtue of the invariance of the equations of elastostatics under the transformation $(\mathbf{X},\mathbf{x}) \rightarrow (k\mathbf{X}, k\mathbf{x})$, relation (12) can then be rewritten as

$$\overline{W}(\overline{\mathbf{F}},c) \geq \frac{1}{|\mathcal{B}|}\int_{\mathcal{B}} W(\mathbf{X},\mathbf{F}^S)\mathrm{d}\mathbf{X} + \overline{\mathbf{P}}\cdot\overline{\mathbf{F}} - \frac{1}{|\mathcal{B}|}\int_{\mathcal{B}} \mathbf{P}\cdot\mathbf{F}^S\mathrm{d}\mathbf{X} \quad (15)$$

where now the volume integrals are not over the entire domain Ω of the CSA but only over the domain $\mathcal{B}$ of a *single* composite sphere. While the second-order tensor $\mathbf{F}^S$ does not correspond to the gradient of a deformation field over Ω in general, the field $\mathbf{P}$ can be selected so that $\mathbf{F}^S$ does correspond to the gradient of a deformation field over each composite sphere. In that case, by invoking once again Hill's lemma, the inequality (15) admits the further simplification

$$\overline{W}(\overline{\mathbf{F}},c) \geq \frac{1}{|\mathcal{B}|}\int_{\mathcal{B}} W(\mathbf{X},\mathbf{F}^S)\mathrm{d}\mathbf{X} + \overline{\mathbf{P}}\cdot\overline{\mathbf{F}} - \overline{\mathbf{P}}\cdot\left[\frac{1}{|\mathcal{B}|}\int_{\mathcal{B}} \mathbf{F}^S\mathrm{d}\mathbf{X}\right] \quad (16)$$

Now, the right-hand side of inequality (16) can be maximized when the constant tensor $\overline{\mathbf{P}}$ is chosen such that

$$\frac{1}{|\mathcal{B}|}\int_{\mathcal{B}} \mathbf{F}^S(\mathbf{X})\mathrm{d}\mathbf{X} = \overline{\mathbf{F}} \quad (17)$$

in which case it reduces finally to

$$\overline{W}(\overline{\mathbf{F}},c) \geq \frac{1}{|\mathcal{B}|}\int_{\mathcal{B}} W(\mathbf{X},\mathbf{F}^S)\mathrm{d}\mathbf{X} \doteq \overline{W}^S(\overline{\mathbf{F}},c) \quad (18)$$

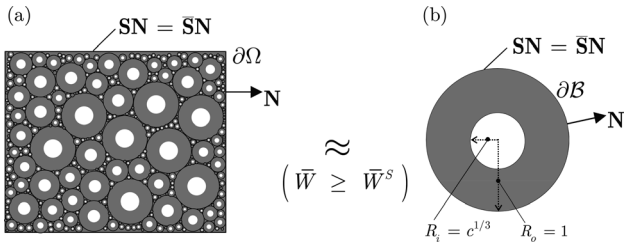

Fig. 2 Schematic illustrating that the overall response of a CSA subjected to affine stress boundary conditions can be variationally approximated by the overall response of a corresponding single composite sphere subjected to the same affine stress boundary conditions. Specifically, the approximation is such that the total elastic energy $\overline{W}$ of the CSA is bounded from below by the total elastic energy $\overline{W}^S$ of the single composite sphere.

In this last expression, again, $\mathcal{B}$ stands for the domain occupied by a single composite sphere with particle concentration c in the undeformed configuration (see Fig. 2(*b*)), $\mathbf{F}^S$ is the deformation gradient tensor defined by the boundary-value problem

$$\mathrm{Div}\left[\frac{\partial W}{\partial \mathbf{F}}(\mathbf{X},\mathbf{F}^S)\right] = 0 \ \text{ in } \ \mathcal{B} \ \text{ and } \ \left[\frac{\partial W}{\partial \mathbf{F}}(\mathbf{X},\mathbf{F}^S)\right]\mathbf{N} = \overline{\mathbf{P}}\mathbf{N} \ \text{ on } \ \partial\mathcal{B} \quad (19)$$

and the constant tensor $\overline{\mathbf{P}}$ is implicitly related to the macroscopic deformation gradient $\overline{\mathbf{F}}$ via

$$\overline{\mathbf{P}} = \frac{1}{|\mathcal{B}|}\int_{\mathcal{B}} \frac{\partial W}{\partial \mathbf{F}}(\mathbf{X},\mathbf{F}^S)\mathrm{d}\mathbf{X} = \frac{\partial \overline{W}^S}{\partial \overline{\mathbf{F}}}(\overline{\mathbf{F}},c) \quad (20)$$

the last equality in (20) stemming from the divergence theorem.

The macroscopic deformation gradient $\overline{\mathbf{F}}$ and effective stored-energy function $\overline{W}^S$ defined by relations (17) and (18) with (19) and (20) constitute the main result of this paper. They characterize—in the form of a variational approximation—the overall nonlinear elastic response of an elastomer, with arbitrary stored-energy function $W^{(1)}$, filled with an isotropic distribution of particles, with arbitrary stored-energy function $W^{(2)}$, of polydisperse sizes and finite concentration c. The following theoretical and practical remarks are in order:

(1) It is plain that the divergence-free field $\mathbf{P}$ devised above is nothing more than a *statically admissible stress field* $\mathbf{S}(\mathbf{X}) = \mathbf{P}(\mathbf{X})$ with prescribed volume average $\overline{\mathbf{S}} = \overline{\mathbf{P}}$ over the entire domain Ω of the CSA. Thus, akin to the classical result in linear elasticity [6], $\overline{W}^S$ corresponds physically to the total elastic energy per unit undeformed volume of a CSA associated with a statically admissible stress field. It is emphasized that the derivation of such a solution, depicted schematically in Fig. 2, without having had to invoke the cumbersome principle of minimum complementary energy in finite elasticity was made possible by the use of the Legendre transformation (7); see Ref. [16] for relevant comments on this approach.

(2) The computation of the overall nonlinear elastic response of filled elastomers, as determined by the above CSA variational approximation, amounts to solving the boundary-value problem (19) for the deformation gradient field $\mathbf{F}^S$ over a single composite sphere $\mathcal{B}$. And then carrying out the volume integrals (17) and (18) to finally compute the macroscopic deformation gradient $\overline{\mathbf{F}}$ and effective stored-energy function $\overline{W}^S$ in terms of the applied macroscopic stress $\overline{\mathbf{S}}(=\overline{\mathbf{P}})$. In general, it is not possible to solve Eq. (19) by analytical means, but it is straightforward to solve it

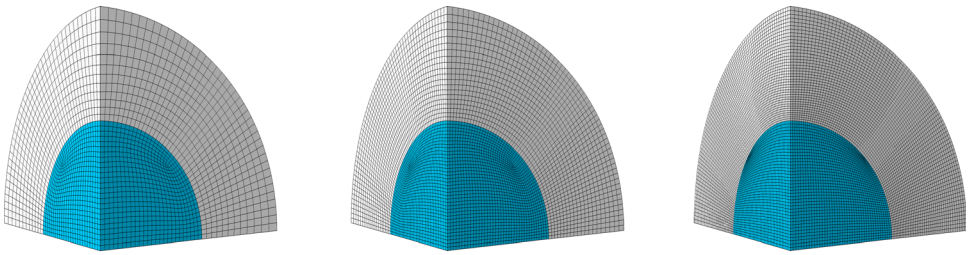

Fig. 3 Three representative meshes in the undeformed configuration for a composite sphere with particle concentration $c = 0.15$: (*a*) coarse mesh with 28,400 elements, (*b*) fine mesh with 102,600 elements, and (*c*) very fine mesh with 260,800 elements

numerically. In the next section, we present an effective finite-element (FE) approach to carry out the calculations.

(3) By construction, the effective stored-energy function $\overline{W}^S$ is an exact result (i.e., the equality holds in (18)) in the dilute limit of particles as $c \to 0+$. As the concentration of particles increases, $\overline{W}^S$ is expected to progressively deviate from $\overline{W}$ providing increasingly softer approximations for the overall response of filled elastomers. This expectation is supported by comparisons with the 3D full-field simulations presented further below in the applications section.

(4) Owing to the proper linearization of the energies $W^{(1)}$ and $W^{(2)}$ of the matrix and particles, the effective stored-energy function $\overline{W}^S$ linearizes properly in the limit of small applied stresses as $\overline{\mathbf{S}} \to \mathbf{0}$ reducing to

$$\overline{W}^S(\overline{\mathbf{F}}, c) = \frac{1}{2}\overline{\varepsilon} \cdot \overline{\mathcal{L}}^S \overline{\varepsilon} + O(\overline{\varepsilon}^3) \tag{21}$$

where $\overline{\varepsilon} = (\overline{\mathbf{F}} + \overline{\mathbf{F}}^T - 2\mathbf{I})/2$ and $\overline{\mathcal{L}}^S = \overline{\mathcal{L}}^S(c)$ stands for the effective modulus tensor of the filled elastomer in its ground state.

(5) For the prominent case when the underlying matrix and particles are constitutively isotropic, it follows that the exact effective stored-energy function $\overline{W}$ is macroscopically isotropic, namely, $\overline{W}(\overline{\mathbf{Q}}\,\overline{\mathbf{F}}\,\overline{\mathbf{Q}}', c) = \overline{W}(\overline{\mathbf{F}}, c)$ for all proper orthogonal second-order tensors $\overline{\mathbf{Q}}$ and $\overline{\mathbf{Q}}'$. In this case, it is not difficult to show that the approximate effective stored-energy function $\overline{W}^S$ has the merit to be functionally exact in that it is identically isotropic; i.e., $\overline{W}^S(\overline{\mathbf{Q}}\,\overline{\mathbf{F}}\,\overline{\mathbf{Q}}', c) = \overline{W}^S(\overline{\mathbf{F}}, c)\ \forall\, \overline{\mathbf{Q}}, \overline{\mathbf{Q}}' \in Orth^+$.

(6) When the underlying matrix and particles are incompressible, the exact macroscopic constraint of incompressibility ensuing from the microscopic constraint $C(\mathbf{X}, \mathbf{F}) = \det \mathbf{F} - 1 = 0 \quad \forall \mathbf{X} \in \Omega$ is given by $C(\overline{\mathbf{F}}, c) = \det \overline{\mathbf{F}} - 1 = 0$ so that $\overline{W}(\overline{\mathbf{F}}, c) = +\infty$ if $\det \overline{\mathbf{F}} \neq 1$. Owing to the lack of separation of length scales between the particle and the surrounding matrix material in the boundary-value problem[3] (19), the resulting approximate macroscopic deformation gradient (17) is not necessarily such that $\det \overline{\mathbf{F}} = 1$ (even though $\det \mathbf{F}^S = 1$ for all $\mathbf{X} \in \mathcal{B}$). Nevertheless, in the broad range of cases that we have examined numerically, the determinant of the resulting $\overline{\mathbf{F}}$ exhibits little deviation from 1.

4 FE Solutions for the Auxiliary Problem of a Single Composite Sphere Under Affine Stresses

In the sequel, we present an FE procedure to construct numerical solutions for the boundary-value problem (19) and average quantities (17) and (18), from which we can then determine the overall response of filled elastomers under general loading conditions. While the above-presented variational approximation applies more generally, for conciseness, attention is restricted here to the physically prominent case of matrix and particles that are *constitutively isotropic*. We begin in Sec. 4.1 by describing the construction of the FE model utilized to carry out the relevant calculations. The description of the numerical method of solution of $\overline{W}^S$ and $\overline{\mathbf{F}}$ for a given $\overline{\mathbf{S}}$ is discussed in Sec. 4.2.

4.1 The FE Model. Without loss of generality, we consider the domains occupied by the matrix ($r = 1$) and particle ($r = 2$) in the composite sphere to be such that

$$\mathcal{B}^{(1)} = \{\mathbf{X} : c^{1/3} \leq |\mathbf{X}| \leq 1\} \quad \text{and} \quad \mathcal{B}^{(2)} = \{\mathbf{X} : |\mathbf{X}| \leq c^{1/3}\} \tag{22}$$

respectively. That is, the center of the composite sphere is placed at the origin of the laboratory Cartesian axes $\{\mathbf{e}_i\}$, and units of length are chosen so that the outer radius $R_o = 1$ while the particle radius is set at $R_i = c^{1/3}$ in terms of the concentration of particles. The geometric and constitutive symmetries of the problem allow performing the calculations in just one octant of the composite sphere. The 3D discretization of such a subdomain is performed with help of a mesh generator code in such a way that radial symmetry is preserved. Eight-node hybrid brick elements—where the pressure is treated as a further degree of freedom in order to be able to handle compressible as well as incompressible constitutive behaviors—are utilized for the analysis. Since the computations are carried out using the FE package ABAQUS, we make use in particular of the C3D8H hybrid elements available in this code [17]. Figure 3 shows three representative meshes of increasing refinement. Mesh sensitivity studies reveal that meshes with approximately 100,000 elements (such as the fine mesh shown in Fig. 3(*b*)) produce sufficiently accurate results, irrespectively of the concentration of particle c.

4.2 Computation of the Overall Response. By virtue of the geometric and constitutive isotropy of the problem, the resulting overall elastic response of the composite sphere is isotropic. This implies that the effective stored-energy function $\overline{W}^S$ in this case depends on the macroscopic deformation gradient $\overline{\mathbf{F}}$ only through its singular values $\overline{\lambda}_1, \overline{\lambda}_2, \overline{\lambda}_3$. More explicitly,

$$\overline{W}^S(\overline{\mathbf{F}}, c) = \overline{\Psi}^S(\overline{\lambda}_1, \overline{\lambda}_2, \overline{\lambda}_3, c) \tag{23}$$

where $\overline{\Psi}^S(\overline{\lambda}_1, \overline{\lambda}_2, \overline{\lambda}_3, c)$ is a symmetric function with respect to its first three arguments.

A further direct implication of the overall isotropy of the problem is that it suffices to consider affine stress boundary conditions of the diagonal form

$$\mathbf{SN} = \overline{\mathbf{S}}\mathbf{N} \quad \text{on} \quad \partial\mathcal{B} \quad \text{with} \quad \overline{\mathbf{S}} = \text{diag}(\overline{s}_1, \overline{s}_2, \overline{s}_3) \tag{24}$$

[3] In other words, the composite sphere is a composite structure and *not* a composite material.

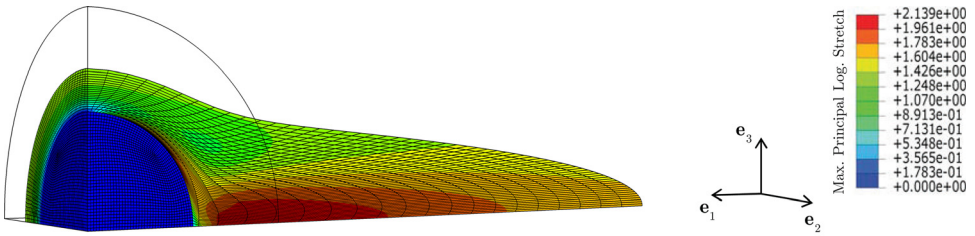

Fig. 4 Contour plots of the maximum principal logarithmic strain for a composite sphere with $c = 0.15$, Neo-Hookean matrix, and 10^4–times stiffer Neo-Hookean particle subjected to affine uniaxial stress (24) with $\bar{\mathbf{S}} = \mathrm{diag}(\bar{s}_1 > 0, 0, 0)$; the undeformed configuration is also depicted for comparison purposes. The overall stretch in the direction of applied stress is $\bar{\lambda}_1 = 3.5$.

since $\bar{s}_i = \partial\overline{\Psi}^S(\bar{\lambda}_1, \bar{\lambda}_2, \bar{\lambda}_3, c)/\partial\bar{\lambda}_i$ $(i = 1, 2, 3)$ in this case. A convenient way to implement these boundary conditions is to follow radial paths in $(\bar{s}_1, \bar{s}_2, \bar{s}_3)$–stress space. Specifically, we set

$$\bar{s}_1 = s\cos\Theta\sin\Phi, \quad \bar{s}_2 = s\sin\Theta\sin\Phi, \quad \bar{s}_3 = s\cos\Phi \tag{25}$$

where s is the monotonically increasing load parameter of the process, which takes the value of 0 in the undeformed stress-free configuration, and $\Theta \in [0, 2\pi]$ and $\Phi \in [0, \pi]$ are the load path angles. Any desired macroscopic stress state $\bar{\mathbf{S}} = \mathrm{diag}(\bar{s}_1, \bar{s}_2, \bar{s}_3)$ can be accessed by marching along (starting at $s = 0$) radial paths (25) with appropriate fixed values of the angles Θ and Φ.

For a given radial path (25), the FE calculations are carried out by gradually increasing the load parameter s from 0 to the desired final value; for the classes of materials to be studied here, the typical step size in the gradual increase of s is $\Delta s = 10^{-2}$. At each step in such a loading path, the incremental equilibrium equations are solved directly in ABAQUS and the integrals (17) and (18) defining the macroscopic deformation gradient $\bar{\mathbf{F}}$ and effective stored-energy function $\overline{W}^S$ computed. It is emphasized that the computational cost of these calculations is low and that very large overall deformations can be achieved. For illustrative purposes, Fig. 4 shows the deformed mesh of a composite sphere for the case of $c = 0.15$, Neo-Hookean matrix, and 10^4 times stiffer Neo-Hookean particle under affine uniaxial stress (24) with $\bar{\mathbf{S}} = \mathrm{diag}(\bar{s}_1 > 0, 0, 0)$. The overall stretch in the direction of applied stress is $\bar{\lambda}_1 = 3.5$. Locally, the deformation is of course even larger (in the matrix) as the contour plots of the maximum principal logarithmic stretch show in the figure.

5 Sample Applications and Discussion

In this section we present a compendium of results for the overall nonlinear elastic response of filled elastomers, as characterized by the CSA formulation described in Sec. 3. Motivated by the properties of typical filled elastomers, attention is restricted to *isotropic incompressible* matrix materials and (approximately) *rigid* filler particles. Results for the linear elastic response in the small-deformation regime are presented first followed by results for the large-deformation response of filled Gaussian (Neo-Hookean) rubber with matrix stored-energy function

$$W^{(1)}(\mathbf{F}) = \begin{cases} \frac{\mu}{2}[\mathbf{F}\cdot\mathbf{F} - 3] & \text{if} \quad \det\mathbf{F} = 1 \\ +\infty & \text{otherwise} \end{cases} \tag{26}$$

The third set of results pertains to the response of a filled rubber wherein the underlying elastomeric matrix is characterized by the non-Gaussian stored-energy function

$$W^{(1)}(\mathbf{F}) = \begin{cases} \dfrac{3^{1-\alpha_1}}{2\alpha_1}\mu_1[(\mathbf{F}\cdot\mathbf{F})^{\alpha_1} - 3^{\alpha_1}] + \dfrac{3^{1-\alpha_2}}{2\alpha_2}\mu_2[(\mathbf{F}\cdot\mathbf{F})^{\alpha_2} - 3^{\alpha_2}] & \text{if} \quad \det\mathbf{F} = 1 \\ +\infty & \text{otherwise} \end{cases} \tag{27}$$

with $\mu_1 = 0.032$ MPa, $\mu_2 = 0.3$ MPa, $\alpha_1 = 3.837$, $\alpha_2 = 0.559$, corresponding to a model that has been shown to accurately describe the nonlinear elastic response of typical silicone rubber over large ranges of deformations (see Sec. 2.3 in Ref. [18]). In all the calculations, the comparatively rigid particles are modeled as incompressible Neo-Hookean solids with stored-energy function

$$W^{(2)}(\mathbf{F}) = \begin{cases} \frac{\mu_p}{2}[\mathbf{F}\cdot\mathbf{F} - 3] & \text{if} \quad \det\mathbf{F} = 1 \\ +\infty & \text{otherwise} \end{cases} \tag{28}$$

where the parameter μ_p is set to be four orders of magnitude larger[4] than the initial shear modulus of the underlying matrix material, namely, $\mu_p = 10^4 \times \mu$ for the case of filled Neo-Hookean rubber and $\mu_p = 10^4 \times (\mu_1 + \mu_2)$ for the case of filled silicone rubber.

[4]The initial shear moduli of standard reinforcing fillers (e.g., silica) are typically four orders of magnitude larger than those of standard elastomers (e.g., silicone).

The selection of results presented here aims at providing further insight into the proposed CSA approach and at assessing its accuracy and numerical efficiency for a broad range of elastomeric matrix materials, particle concentrations, and loading conditions. To aid in this process, the CSA results are confronted with the recent 3D full-field simulations of Lopez-Pamies et al. [19]. These are finite-element simulations of the large-deformation response of elastomers reinforced by random isotropic distributions of rigid spherical particles with the same (monodisperse) and with different (polydisperse) sizes. For the values of particle concentration considered here, the dispersion in the size of the particles turns out not to have an effect on the overall response of the simulations (see Sec. 6 in Ref. [19]). Accordingly, no distinction is made henceforth of whether the presented full-field FE simulations are for monodisperse or for polydisperse microstructures.

5.1 Linear Elastic Results. In the limit of small deformations (see remark 4 in Sec. 3.2), for the case of isotropic incompressible matrix materials and rigid particles, the CSA stored-energy function (18) reduces to

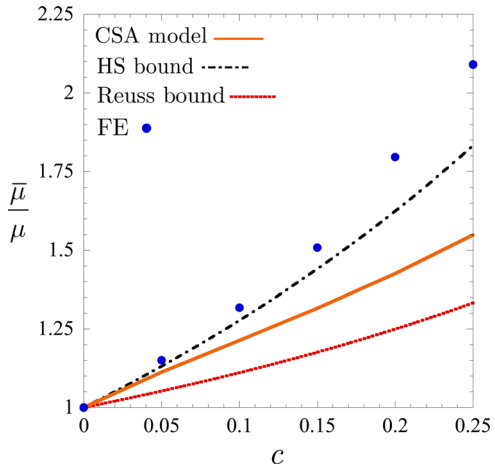

Fig. 5 The normalized initial effective shear modulus $\overline{\mu}/\mu$ of isotropic incompressible elastomers filled with random isotropic distributions of rigid particles. Plots are shown for: (*i*) the CSA approximation $\overline{\mu}^S$, (*ii*) full-field FE simulations, (*iii*) the Hashin–Shtrikman lower bound $\overline{\mu}^{HS}/\mu = (2+3c)/(2-2c)$, and (*iv*) the Reuss lower bound $\overline{\mu}^R/\mu = 1/(1-c)$, as functions of the concentration of particles *c*.

$$\overline{W}^S(\overline{\mathbf{F}}, c) = \overline{\mu}^S\left[\overline{\varepsilon}_1^2 + \overline{\varepsilon}_2^2 + \overline{\varepsilon}_3^2\right] \quad \text{with} \quad \overline{\varepsilon}_1 + \overline{\varepsilon}_2 + \overline{\varepsilon}_3 = 0 \tag{29}$$

to leading order in the deformation measures $\overline{\varepsilon}_i = \overline{\lambda}_i - 1$ $(i = 1, 2, 3)$, where it is recalled that $\overline{\lambda}_i$ denote the singular values of the macroscopic deformation gradient $\overline{\mathbf{F}}$ and $\overline{\mu}^S$ stands for the initial effective shear modulus of the filled rubber. Figure 5 presents plots for $\overline{\mu}^S$, normalized by the initial shear modulus μ of the underlying elastomeric matrix, as a function of the concentration of particles c. Results are also presented for the corresponding full-field FE simulations for isotropic distribution of rigid spherical particles, as well as for the Hashin–Shtrikman and Reuss lower bounds for the effective shear modulus of rigidly reinforced, isotropic, incompressible, linearly elastic materials.

Two plain observations from Fig. 5 are that the CSA result stiffens monotonically with increasing values of c, as expected on physical grounds, and that it is in good quantitative agreement with the full-field FE simulations for concentrations up to about $c = 0.05$, remaining softer thereafter. This latter behavior is consistent with the fact the CSA result is exact in the dilute limit of particles as $c \to 0+$, but a lower bound for finite values of c (see remark 3 in Sec. 3.2). More specifically, the CSA result is seen to be consistently stiffer than the Reuss bound but *softer* than the corresponding Hashin–Shtrikman bound beyond $c = 0.05$.

5.2 Results for Filled Neo-Hookean Rubber. Having examined the small-deformation regime, we now turn to consider the response of filled elastomers under arbitrarily large deformations. We begin by considering the basic case of filled Neo-Hookean rubber. Figure 6 shows results for the effective stored-energy function of Neo-Hookean rubber reinforced by an isotropic distribution of rigid particles of concentration $c = 0.15$. Figure 6(*a*) displays the entire energy function in terms of the macroscopic principal stretches $\overline{\lambda}_1$ and $\overline{\lambda}_2$, whereas 6(*b*) displays the cross section of the energy along the axisymmetric deformation plane with $\overline{\lambda}_1 = \overline{\lambda}_2 = \overline{\lambda}$. Results are shown for the CSA approximate energy $\overline{W}^S$ in both parts of the figure and for the corresponding full-field FE simulations for isotropic distributions of spherical particles in 6(*b*).

A key point to emphasize from Fig. 6 is that the construction of the *entire* CSA effective stored-energy function $\overline{W}^S$ over *large ranges* of macroscopic deformations $\overline{\mathbf{F}}$ —which, again, serves to characterize the macroscopic constitutive response of the filled elastomer under general loading conditions via Eq. (20)—is straightforward and computationally inexpensive. Another key point is that the CSA approximation is in good agreement with the full-field FE simulations in the large-deformation regime, even at the relatively high value of particle concentration $c = 0.15$.

To gain more precise insight into the accuracy and range of validity of the CSA approximation, Fig. 7 presents results for the large-deformation response of filled Neo-Hookean rubber for particle concentrations of $c = 0.05$ and 0.15 under: 7(*a*) uniaxial compression, 7(*b*) uniaxial tension, 7(*c*) pure shear, and 7(*d*) simple shear. The constitutive stress-deformation relations for these loading conditions in terms of the effective stored-energy function $\overline{W}^S$ read explicitly as

- *Uniaxial loading* ($\overline{\lambda}_1 = \overline{\lambda}, \overline{\lambda}_2 = \overline{\lambda}_3 = \overline{\lambda}^{-1/2}$ with $\overline{s}_2 = \overline{s}_3 = 0$):

$$\overline{S}_{un} = \frac{\mathrm{d}\overline{W}^S}{\mathrm{d}\overline{\lambda}} \tag{30}$$

- *Pure shear* ($\overline{\lambda}_1 = \overline{\lambda}, \overline{\lambda}_2 = \overline{\lambda}^{-1}, \overline{\lambda}_3 = 1$ with $\overline{s}_2 = 0$):

$$\overline{S}_{ps} = \frac{\mathrm{d}\overline{W}^S}{\mathrm{d}\overline{\lambda}} \tag{31}$$

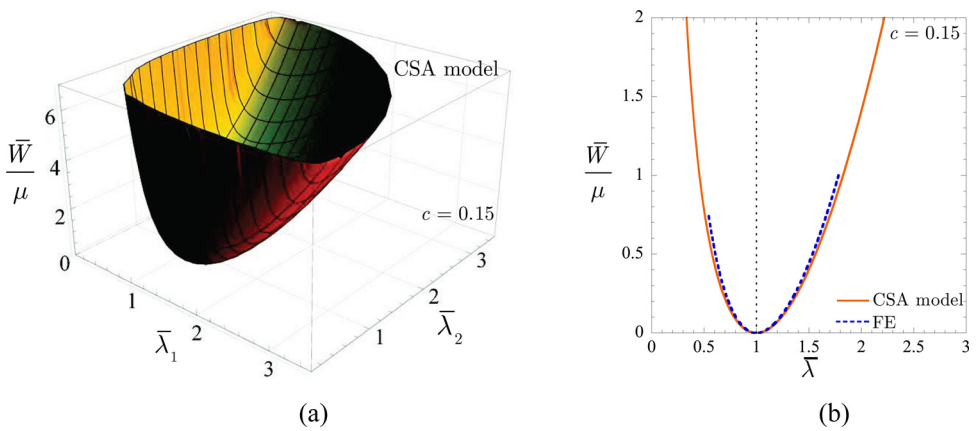

Fig. 6 Macroscopic response of Neo-Hookean rubber filled with an isotropic distribution of rigid particles of concentration $c = 0.15$. Part (*a*) displays the entire effective stored-energy function in terms of the macroscopic principal stretches $\overline{\lambda}_1$ and $\overline{\lambda}_2$, whereas part (*b*) shows the energy along axisymmetric loading conditions with $\overline{\lambda}_1 = \overline{\lambda}$, $\overline{\lambda}_2 = \overline{\lambda}^{-1/2}$. Results are shown for the CSA approximation $\overline{W}^S$ in both parts, and for corresponding full-field FE simulations for isotropic distributions of spherical particles in part (*b*).

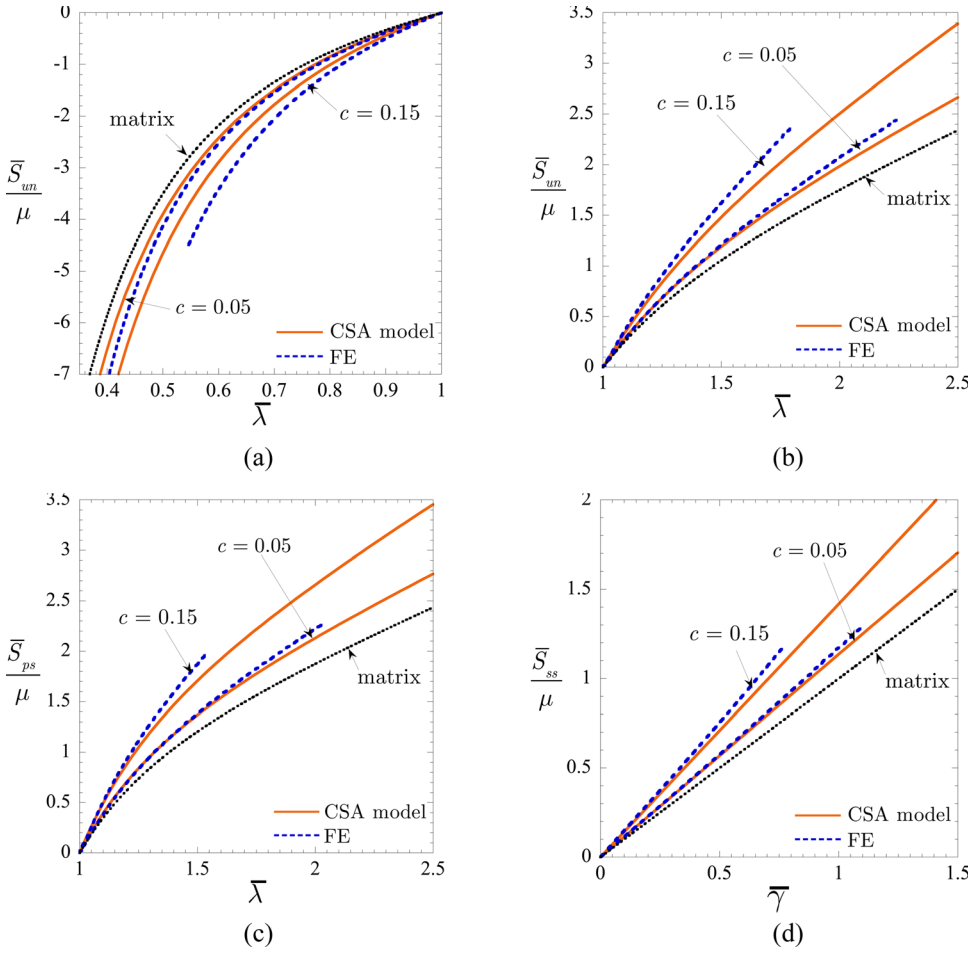

Fig. 7 Macroscopic response of filled Neo-Hookean rubber with various values of concentration of particles *c* under: (*a*) uniaxial compressive, (*b*) uniaxial tensile, (*c*) pure shear, and (*d*) simple shear loading conditions. Plots are shown for the CSA approximation and corresponding full-field FE simulations for isotropic distributions of spherical particles.

- *Simple shear* ($\overline{\lambda}_1 = (\overline{\gamma} + \sqrt{\overline{\gamma}^2 + 4})/2$, $\overline{\lambda}_2 = \overline{\lambda}_1^{-1}$, $\overline{\lambda}_3 = 1$):

$$\overline{S}_{ss} = \frac{\mathrm{d}\overline{W}^S}{\mathrm{d}\overline{\gamma}} \tag{32}$$

where $\overline{S}_{un}$, $\overline{S}_{ps}$, $\overline{S}_{ss}$ denote first Piola–Kirchhoff stress measures. The corresponding full-field FE results for isotropic distributions of spherical particles are also plotted in the figure.

In addition to the monotonic stiffening of the response for increasing values of particle concentration, it is immediate from Fig. 7 that the CSA and FE results are in fairly good qualitative and quantitative agreement for all loading conditions. As expected from the variational construction of the CSA formulation (see remark 3 in Sec. 3.2), the agreement is better for the case of the smaller concentration $c = 0.05$ but remains remarkably good for the relatively high concentration $c = 0.15$, with a maximum difference of about 15% occurring along uniaxial compression. Figure 7 also serves to illustrate the fact that the CSA approach allows reaching much larger overall deformations than those achieved with full-field simulations.

5.3 Results for a Filled Silicone Rubber. Figure 8 presents various results for the large-deformation response of a filled non-Gaussian rubber, wherein the underlying matrix material is a typical silicone rubber characterized here by the stored-energy function (27) with material parameters $\mu_1 = 0.032$ MPa, $\mu_2 = 0.3$ MPa, $\alpha_1 = 3.837$, $\alpha_2 = 0.559$. Figs. 8(*a*)–8(*d*) show the macroscopic stress-deformation relation for uniaxial compression, uniaxial tension, pure shear, and simple shear for particle concentrations $c = 0.05$ and 0.15. Results are shown for the CSA approximation and for the corresponding full-field FE simulations.

Akin to all previous results, the overall constitutive response of the filled elastomer is seen to stiffen for increasing values of particle concentration. Similar to the Neo-Hookean case, here the CSA results also exhibit good qualitative and quantitative agreement with the full-field FE simulations for all loading conditions. The largest discrepancy occurs, again, along uniaxial compressive loading for the largest concentration of particles $c = 0.15$.

In short, the above three sets of sample results indicate that the proposed CSA formulation provides a numerically efficient, functionally sound, and quantitatively fairly accurate approach to compute the overall nonlinear elastic response of isotropic filled elastomers, with small-to-moderate concentration of particles, under arbitrarily large deformations.

6 Final Remarks: Generalizations

The variational method proposed in this work constitutes a powerful platform from which to account for more levels of complexity to model soft solids with particulate microstructures. Below, we discuss some of these generalizations.

6.1 Anisotropic Distributions of Particles of Anisotropic Shape. Recent experimental studies have revealed (see, e.g., Chapter 6 in Refs. [8] and [9]) that anisotropic distributions of

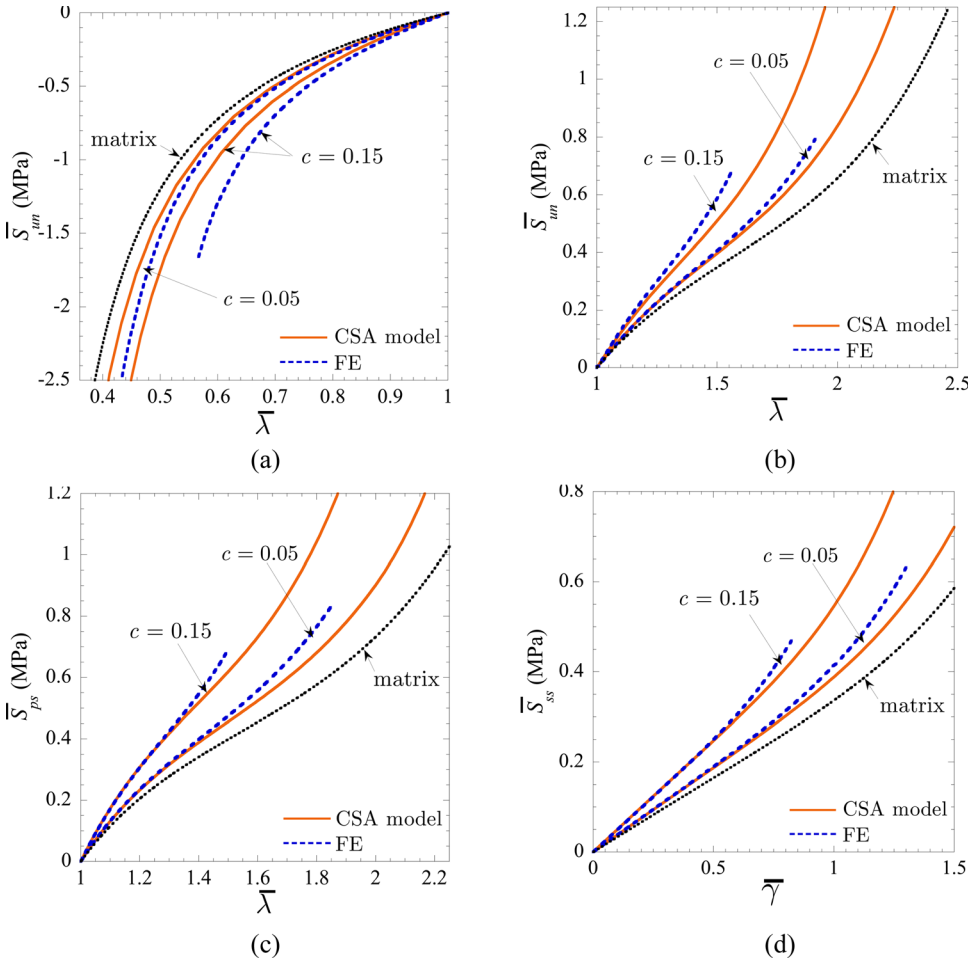

Fig. 8 Macroscopic response of filled silicone rubber with various values of concentration of particles *c* under: (*a*) uniaxial compressive, (*b*) uniaxial tensile, (*c*) pure shear, and (*d*) simple shear loading conditions. Plots are shown for the CSA approximation and corresponding full-field simulations for isotropic distributions of spherical particles.

fillers, such as for instance the chainlike distributions shown in Fig. 9(*a*), may serve to enhance certain multifunctional properties of filled elastomers, including their electro- and magnetostriction capabilities. These—and even more complex—microstructures can be idealized as assemblages of composite ellipsoids, wherein the filler particle can be chosen of any required anisotropic shape (not necessarily ellipsoidal). Figure 9(*b*) depicts schematically the case of a composite-ellipsoid assemblage (CEA) of nonspherical particles; all the ellipsoids in the assemblage are scaled-up or scaled-down versions of each other (see, e.g., Chapter 7 in Refs. [15] and [20]).

It is a simple matter to show that the formulation presented in Sec. 3.2 for CSAs is actually applicable more generally to CEAs—with the domain $\mathcal{B}$ then denoting the single composite ellipsoid of interest. The variational framework Eqs. (17)–(20) provides, thus, a numerically efficient means to bottom-up model the overall nonlinear elastic response of elastomers filled with general classes of anisotropic distributions of particles of anisotropic shapes under arbitrarily large deformations.

6.2 Bound Rubber. It is by now well established that the presence of bound rubber—namely, the interphasial material

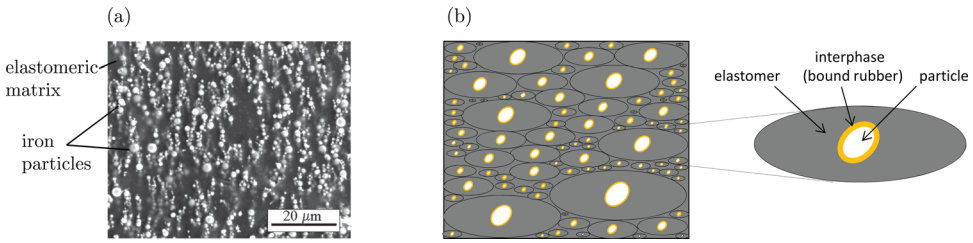

Fig. 9 (*a*) Electron micrograph of a magnetorheological elastomer with iron particles distributed anisotropically in chainlike structures [9] and (*b*) its idealization as an ellipsoidal assemblage of possibly nonspherical particles (CEA). All the composite ellipsoids in the assemblage are homothetic in that they are scaled-up or scaled-down versions of each other. Part (*b*) also illustrates schematically the straightforward incorporation of bound rubber into the CEA idealization.

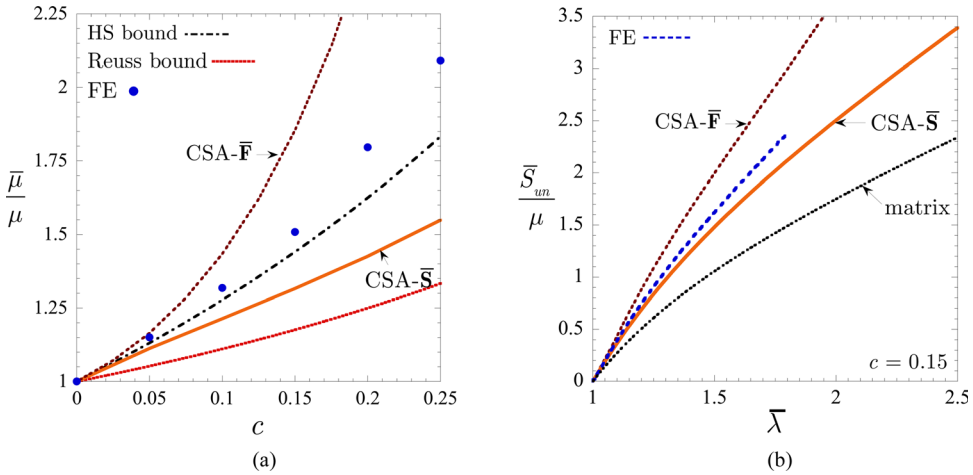

Fig. 10 Comparisons between the kinematically admissible approximation (A1) and (A2), denoted as CSA-$\overline{\mathbf{F}}$, and the statically admissible approximation Eqs. (17)–(20), denoted as CSA-$\overline{\mathbf{S}}$, for the overall response of filled Neo-Hookean rubber. Part (*a*) shows results for the normalized initial shear modulus $\overline{\mu}/\mu$ as a function of particle concentration c, while part (*b*) shows stress-deformation results for $c = 0.15$ under uniaxial tension.

surrounding the fillers—contributes significantly to the overall stiffness of filled elastomers (see, e.g., Ref. [1] and references therein; see also Ref. [21]). It is typically several tens of nanometers in width, constitutively heterogeneous, and markedly stiffer than the elastomeric matrix in the bulk (see, e.g., Refs. [14,22]). Very little attention has been paid to the incorporation of this mechanism into the microscopic modeling of filled elastomers, especially at large deformations, presumably because of the intrinsic technical difficulties.

The formulation presented in Sec. 3.2 can be readily extended to account for the presence of bound rubber (and other filler-elastomer interphasial phenomena) in filled elastomers. The idea is to consider a CSA—or, more generally, a CEA—where the filler particles are bonded to the elastomeric matrix through an interphase, possibly of finite size, anisotropic shape, and constitutively heterogeneous. This is shown schematically in Fig. 9(*b*).

Acknowledgment

Support for this work by the National Science Foundation through the CAREER Grant CMMI–1055528 and by the Civil and Environmental Engineering Department at the University of Illinois Urbana-Champaign through the CEE Innovation Grant Program is gratefully acknowledged.

Appendix: Kinematically Admissible Approximation for the Response of a CSA

Following a parallel reasoning to that presented in Sec. 3.2, it is not difficult to deduce that

$$\overline{W}(\overline{\mathbf{F}},c) \leq \frac{1}{|\mathcal{B}|}\int_{\mathcal{B}} W(\mathbf{X},\mathbf{F}^K)\mathrm{d}\mathbf{X} \doteq \overline{W}^K(\overline{\mathbf{F}},c) \qquad \text{(A1)}$$

where the deformation gradient field $\mathbf{F}^K$ is defined implicitly by the boundary-value problem

$$\mathrm{Div}\left[\frac{\partial W}{\partial \mathbf{F}}(\mathbf{X},\mathbf{F}^K)\right] = 0 \quad \text{in} \quad \mathcal{B} \quad \text{and} \quad \mathbf{x} = \overline{\mathbf{F}}\mathbf{X} \quad \text{on} \quad \partial\mathcal{B} \qquad \text{(A2)}$$

The effective stored-energy function $\overline{W}^K$ corresponds physically to the total elastic energy per unit undeformed volume of a CSA associated with a kinematically admissible field—one in which every composite sphere satisfies the equilibrium equations in its interior and is subjected to the affine deformation $\mathbf{x} = \overline{\mathbf{F}}\mathbf{X}$ on its boundary.

Much like $\overline{W}^S$, the effective stored-energy function $\overline{W}^K$ is by construction an exact result (i.e., the equality holds in Eq. (A1)) in the dilute limit of particles as $c \to 0+$. As c increases, $\overline{W}^K$ is expected to deviate from $\overline{W}$ providing increasingly stiffer approximations for the overall response of filled elastomers. For the case of interest here when the particles are much stiffer than the elastomeric matrix, this deviation is exceedingly drastic leading to overly stiff approximations. Figure 10 illustrates this behavior for the case of filled Neo-Hookean rubber. Fig. 10(*a*) displays results for the normalized initial effective shear modulus $\overline{\mu}/\mu$ in the small deformation regime as a function of particle concentration c, while A1(*b*) shows results for the stress-deformation relation for $c = 0.15$ under uniaxial tensile loading conditions.

References

[1] Leblanc, J. L., 2010, *Filled Polymers: Science and Industrial Applications*, CRC Press, Boca Raton, FL.
[2] Smallwood, H. M., 1944, "Limiting Law of the Reinforcement of Rubber," J. Appl. Phys., **15**, pp. 758–766.
[3] Guth, E., 1945, "Theory of Filler Reinforcement," J. Appl. Phys., **16**, pp. 20–25.
[4] Hill, R., 1972, "On Constitutive Macrovariables for Heterogeneous Solids at Finite Strain," Proc. R. Soc. Lond. A, **326**, pp. 131–147.
[5] Lopez-Pamies, O., Goudarzi, T., and Nakamura, T., 2013, "The Nonlinear Elastic Response of Suspensions of Rigid Inclusions in Rubber: I—An Exact Result for Dilute Suspensions," J. Mech. Phys. Solids, **61**, pp. 1–18.
[6] Hashin, Z., 1962, "The Elastic Moduli of Heterogeneous Materials," ASME J. Appl. Mech., **29**, pp. 143–150.
[7] Barrett, K. E., and Talbot, D. R. S., 1996, "Bounds for the Effective Properties of a Nonlinear Two-Phase Composite Dielectric," Proc. 8th Int. Symp. Continuum Models and Discrete Systems, Varna, Bulgaria, June 11–16, 1995, World Scientific, Singapore.
[8] Carpi, F., De Rossi, D., Kornbluh, R., Pelrine, R., and Sommer-Larsen, P., 2008, *Dielectric Elastomers as Electromechanical Transducers*, Elsevier, New York.
[9] Danas, K., Kankanala, S. V., and Triantafyllidis, N., 2012, "Experiments and Modeling of Iron-Particle-Filled Magnetorheological Elastomers," J. Mech. Phys. Solids, **60**, pp. 120–138.
[10] Ogden, R. W., 1978, "Extremum Principles in Non-Linear Elasticity and Their Application to Composites—I Theory," Int. J. Solids. Struct., **14**, pp. 265–282.
[11] Lee, S. J., and Shield, R. T., 1980, "Variational Principles in Finite Elastostatics, J. Appl, Math. Phys., **31**, pp. 437–453.
[12] Khisaeva, Z. F., and Ostoja-Starzewski, M., 2006, "Mesoscale Bounds in Finite Elasticity and Thermoelasticity of Random Composites," Proc. R. Soc. Lond. A, **462**, pp. 1167–1180.
[13] Ogden, R. W., 1997, *Non-Linear Elastic Deformations*, Dover Publications, Mineola, NY.
[14] Ramier, J., 2004, "Comportement Mécanique d'élastomérs Chargés, Influence de l'adhésion Charge–Polymére, Influence de la Morphologie," Ph. D. dissertation, Institut National des Science Appliquées de Lyon, France.

[15] Milton, G. W., 2002, *The Theory of Composites* (Cambridge Monographs on Applied and Computational Mathematics, Vol. 6), Cambridge University Press, Cambridge, UK.
[16] Willis, J. R., 1989, "The Structure of Overall Constitutive Relations for a Class of Nonlinear Composites, IMA J. Appl. Math., **43**, pp. 231–242.
[17] Dassault Systemes Simulia Corp., 2011, ABAQUS Version 6.11 Documentation, Providence, RI.
[18] Lopez-Pamies, O., 2010,"A New I_1-Based Hyperelastic Model for Rubber Elastic Materials," Comptes Rendus Mecanique, **338**, pp. 3–11.
[19] Lopez-Pamies, O., Goudarzi, T., and Danas, K., 2013, "The Nonlinear Elastic Response of Suspensions of Rigid Inclusions in Rubber: II—A Simple Explicit Approximation for Finite-Concentration Suspensions," J. Mech. Phys. Solids, **61**, pp. 19–37.
[20] Bornert, M., Stolz, C., and Zaoui, A., 1996, "Morphologically Representative Pattern-Based Bounding in Elasticity," J. Mech. Phys. Solids, **44**, pp. 307–331.
[21] Bertoldi, K., and Lopez-Pamies, O., 2012, "Some Remarks on the Effect of Interphases on the Mechanical Response and Stability of Fiber-Reinforced Elastomers," ASME J. Appl. Mech., **79**, p. 031023.
[22] Qu, M., Deng, F., Kalkhoran, S. M., Gouldstone, A., Robisson, A., and Van Vliet, K. J., 2011, "Nanoscale Visualization and Multiscale Mechanical Implications of Bound Rubber Interphases in Rubber-Carbon Black Nanocomposites," Soft Matter, **7**, pp. 1066–1077.